

# Charging Process and Coulomb-Force-Directed Printing of Nanoparticles with Sub-100-nm Lateral Resolution

Chad R. Barry, Jie Gu, and Heiko O. Jacobs\*

*Department of Electrical and Computer Engineering, University of Minnesota,  
200 Union Street SE, Minneapolis, Minnesota 55455*

*Received June 24, 2005; Revised Manuscript Received August 12, 2005*

## ABSTRACT

This article reports on a new charging process and Coulomb-force-directed assembly of nanoparticles onto charged surface areas with sub-100-nm resolution. The charging is accomplished using a flexible nanostructured thin silicon electrode. Electrical nanocontacts have been created as small as 50 nm by placing the nanostructured electrode onto an electret surface. The nanocontacts have been used to inject charge into 50 nm sized areas. Nanoparticles were assembled onto the charge patterns, and a lateral resolution of 60 nm has been observed for the first time. A comparison of the nanoparticle patterns with the surface potential distribution recorded by Kelvin probe force microscopy (KFM) revealed a mismatch in the lateral resolution. One possible explanation is that nanoparticles may visualize charge patterns at a sub-60-nm length scale that is not well resolved using KFM.

Inorganic, metallic, and semiconducting nanomaterials in the form of nanoparticles, nanowires, nanobelts, or nanodisks are considered key building blocks in the design of novel high-performance nanotechnological devices. The process to fabricate such devices, however, will require new additive concepts to integrate, orient, and assemble such building blocks at desired locations on a substrate. Current approaches that address the integration of nanomaterials at desired locations on a substrate include serial scanning probe based concepts to print<sup>1,2</sup> or manipulate<sup>3</sup> nanomaterials at the sub-100-nm length scale, semiparallel inkjet-based concepts<sup>4,5</sup> to print materials from suspensions with 10  $\mu\text{m}$  scale resolution, parallel nanotransfer methods<sup>6,7</sup> to transfer nanomaterials from one substrate to another retaining a copy of the order, and a vast variety of programmable or “receptor based” assembly concepts<sup>8–18</sup> that use unordered nanomaterials as an input. Scanning probe and inkjet-based methods enable rapid reconfiguration of the patterns and the formation of heterogeneous assemblies at an early stage but remain too slow to print materials over large areas at the sub-10- $\mu\text{m}$  length scale. Nanotransfer concepts are most suitable to transfer nanomaterials from one substrate to another over large areas. Nanotransfer maintains the arrangement of the nanomaterials on a donor substrate; i.e., it does not order or rearrange the materials as part of the process.

“Receptor”-based concepts focus on the directed assembly of randomly oriented nanomaterials. The materials are suspended in solution or gas phase and are assembled at desired locations (receptors) on a substrate using specific interactions. Most actively investigated areas, currently, use protein recognition,<sup>19,20</sup> DNA hybridization,<sup>9,21,22</sup> hydrophobicity/hydrophilicity, surface tension and self-assembled monolayers,<sup>10</sup> topography-directed concepts,<sup>23–25</sup> magnetic<sup>11</sup> and dielectrophoretic assembly and transport,<sup>22,26–28</sup> and electrostatic forces.<sup>12–18,25,27</sup>

In recent years there has been an increased focus on the use of long range electrostatic forces to direct the assembly of nanomaterials since it can potentially be used to assemble a vast variety of materials (magnetic, nonmagnetic, insulating, semiconducting, conducting, organic, and inorganic materials) without altering the surface chemistry of the materials.<sup>12–18,25,27</sup> Electrostatic forces are sufficiently long range to attract nanomaterials from the gas and liquid phases. The other advantage is that global fields can be applied using electrical electrodes to program the assembly.<sup>22</sup> In our own research we have developed a parallel charge patterning process enabling nanoxerographic printing.<sup>12–15</sup> Patterning of charge with 100–200 nm resolution and transfer of 50 nm to 20  $\mu\text{m}$  sized particles including silver, gold, indium, iron oxide, graphitized carbon, iron beads, and Xerox toner from a powder, gas, and liquid phase<sup>12–15</sup> has been accomplished.

\* Corresponding author: hjacobs@umn.edu.

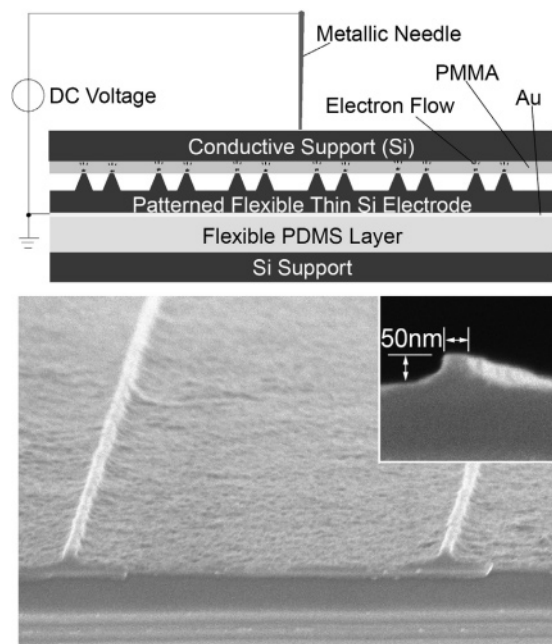


**Figure 1.** (Top) Principle of the electric nanocontact printing process: A silicon chip carrying a thin film electret is placed on top of a thin silicon electrode supported by a flexible PDMS layer on a standard silicon wafer. A needle, attached to a micromanipulator is used to form an electric contact to the backside of the silicon chip. An external voltage is used to transfer a pattern of charge into the electret material at the areas of contact. The silicon chip is removed with the electret carrying a charge pattern. (Bottom) Scanning electron microscope images of the fabricated thin silicon structures.

In this paper we report on a new flexible electrode structure that can form sub-100-nm sized electrical nanocontacts by mechanical placement of the electrode structure on a second surface. The electrical nanocontacts that are established at the interface have been used to inject charge patterns in a dielectric thin film at a resolution that exceeds prior parallel methods.<sup>12,13</sup> We refer to this process as electric nanocontact printing of charge. After the electrode is removed, the charge pattern is used to direct the assembly of nanoparticles from the gas phase. For the first time we observe that 5–40 nm sized nanoparticles have been captured from the gas phase with 60 nm lateral resolution. Kelvin probe force microscopy (KFM) studies have been performed to characterize the surface charge patterns. A comparison of the electrode structure dimensions, the patterns of assembled nanoparticles, and the surface potential distribution recorded by KFM suggest that nanoparticles may be able to visualize charge patterns at the sub-60-nm length scale which is not well resolved using KFM. The results also illustrate that Coulomb forces provide a clear route to the directed assembly of sub-10-nm components onto target areas with sub-100-nm lateral resolution.

The electric nanocontact printing process that has been developed to generate charge patterns is illustrated in Figure 1. It makes use of a flexible, thin silicon electrode to accomplish higher resolution charge transfer than what has been possible with previous methods that were based on metal-coated poly(dimethylsiloxane) (PDMS) stamps.<sup>12,13</sup>

Prior electrode structures tended to collapse for features less than 100 nm in size. The new electrode was made from a 2 in. diameter, 10  $\mu\text{m}$  thick, double-side polished silicon wafer (Virginia Semiconductors). In this study we used an n-doped silicon wafer with a resistivity of 1.3  $\Omega\text{ cm}$ ; p-doped wafers worked as well.

A rigid 500  $\mu\text{m}$  thick silicon wafer coated with a 5 mm layer of PDMS serves as a flexible support for the thin silicon electrode during the fabrication and charging. The PDMS support was coated with a 50 nm thick layer of gold by thermal evaporation to provide electrical conductivity to the backside of the thin silicon wafer. The thin silicon electrode itself is sufficiently conductive and therefore does not require a metal coating on the front side.

The topographical features in the thin silicon electrodes were generated using phase-shift photolithography<sup>29</sup> and reactive-ion etching. In brief, PDMS stamps with 1  $\mu\text{m}$  wide and 400 nm deep surface relief patterns were placed on the thin silicon surface after it was coated with a 500 nm thick Shipley 1805 photoresist and baked at 105  $^{\circ}\text{C}$  for 2 min. The surface was exposed with  $\sim 436$  nm UV light for 1.5 s (Karl Suss MA-6 aligner) and developed in (1:5) volume ratio solution of 351 developer and  $\text{H}_2\text{O}$  for 40 s. The resulting photoresist features are 100 nm wide lines and rings that are 150 nm high. The features are then transferred into the thin silicon substrate by reactive-ion etching for 45 s in a 98%  $\text{CF}_6$ , 2%  $\text{O}_2$  plasma. The etching rate of 1805 within the plasma is 100 nm/min while the etching rate of silicon is 75 nm/min. Therefore, in 45 s, a feature with a height of 50–60 nm is produced in the thin silicon substrate. Due to the removal of photoresist from both the top and the sides, the width of the produced pattern on the silicon surface continuously shrinks during etching and results in tapered silicon structures. The etching time is limited to less than 1 min in order to avoid completely removing the photoresist and thus generating a rough surface. The remaining photoresist is stripped off by acetone and reactive ion etching in oxygen plasma (320 STS etcher) for 120 s. Piranha ( $\text{H}_2\text{SO}_4$ :  $\text{H}_2\text{O}_2 = 2:1$ ) is then dropped on the silicon surface for 2–3 min to completely remove any photoresist residue. The final tapered silicon structures were 50 nm wide at the surface and 50 nm tall (Figure 1).

As the charge storage medium, we used a 60 nm thick film of PMMA on  $\langle 100 \rangle$  p-doped silicon wafers. The film was formed by spin coating a 2% solution of 950 K (PMMA) in chlorobenzene (MicroChem Co.) at 5000 rpm and baking it on a hot plate at 170  $^{\circ}\text{C}$  for 3 min. The chips were placed on the flexible electrode by hand and contacted from the back with a metallic needle attached to a micromanipulator. The micromanipulator was used to adjust the needle's position and to provide pressure to establish contact between the electrode and PMMA thin film. An external voltage was applied for 30 s to generate a constant current of 1–5 mA. After exposure, we removed and characterized the charge patterns using Kelvin probe force microscopy (KFM).<sup>30,31</sup>

Since charge is trapped at the exposure area, a charge pattern matching the pattern on the electrode will remain on the PMMA surface. The nanoxerographic process used to

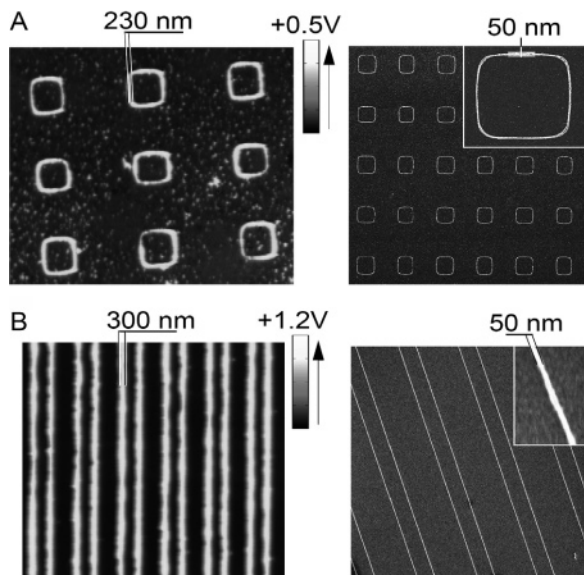


**Figure 2.** Kelvin probe force microscope images (left) of the surface potential distribution of a substrate and scanning electron microscope images (right) of the thin silicon electrode used to pattern the substrate. (A) 230 nm wide patterns of positive charge generated from an electrode containing 50 nm wide square shaped rings. (B) 300 nm wide line patterns of positive charge generated using an electrode containing 50 nm wide structures.

direct the assembly of nanoparticles onto the charge patterned chips has been described in detail elsewhere.<sup>14,15</sup> The process involves the use of a tube furnace system that generates nanoparticles in the gas phase by evaporation and condensation. An argon carrier gas transports the particles out of the furnace and into the particle assembly module. The assembly module consists of a cavity that holds the sample, two electrodes to generate a global electric field, and an electrometer to count the charge of the assembled particles. The global electric field directs incoming charged particles of selected polarity toward the sample surface, where the local electrostatic force takes over and assembles the particles onto the charge patterned areas.

Figure 2 illustrates representative patterns of localized charge in PMMA (left images) that have been patterned using thin silicon electrodes (right images). The images show that charge has been transferred at the contact areas; the local potential increase due to trapped charge was 500 mV in Figure 2A and 1.2 V in Figure 2B. We note that the width of the surface potential distribution 230 and 300 nm is much wider than the width of the feature size on the electrode structure. There are three mechanisms that could cause this mismatch:

First, the tip geometry and condition could affect the surface potential distribution that is recorded by KFM. The influence of the tip geometry on the potential distribution has been calculated previously.<sup>32</sup> The measured distribution is a two-dimensional convolution of the actual surface potential distribution with the transfer function of the tip. Even a single elementary charge will be imaged as a bell curve that is 50–100 nm wide.<sup>32</sup> To the best of our knowledge it has not been possible to accurately resolve the

surface potential distribution of embedded charge patterns in continuous films at the sub-100-nm length scale using Kelvin probe force microscopes that are operated in air at ambient pressure and humidity. We used a Digital Instruments Multimode Nanoscope IV AFM.

Second, the trapped charges could laterally diffuse to form wider lines due to electrostatic repulsion of trapped charge carriers themselves, the reordering of dipoles, ions, or ionic vacancies, and recombination. It is possible to estimate the number of charges and the electrostatic repulsion between individual charges. The trapped charge density can be estimated from the recorded surface potential distribution. Trapped charge inside the PMMA film will attract mobile charge carriers inside the silicon substrate, resulting in the formation of a double layer. For a double layer separated by a distinct distance  $d$ , the projected charge density  $\sigma$  can be calculated with  $\sigma = \epsilon \Delta V/d$ , where  $\epsilon$  is the permittivity, and  $\Delta V$  is the voltage drop across the layer.<sup>33</sup> For  $\epsilon = 2 \times 10^{-11}$  C/(V m) (the approximate permittivity of PMMA),  $\Delta V = 1.2$  V (maximum measured potential change), and  $d = 60$  nm (assumed intermediate distance between the counter charges), we obtain a first-order estimate of the effective charge density of  $\sigma_{\text{eff}} = 30$  elementary charges per surface area of 100 nm by 100 nm. The actual value might range anywhere between  $\sigma_{\text{eff}} = 30$ –100 elementary charges per surface area of 100 nm by 100 nm. The upper value takes into account that the measured surface potential is not recorded accurately at the 100 nm length scale. The measured values for 100 nm sized features are typically a factor of 2–4 lower than the true surface potential. The actual value depends on the tip geometry and scan height.<sup>32</sup>

On the basis of the smallest estimated spacing between trapped charge carriers, 10 nm if we consider a high charge concentration and a homogeneous distribution across the surface, we can compute an upper limit for the repulsive force and energy and compare it with the ionization and polarization energy of PMMA. Considering two elementary charges that are separated by 10 nm, we obtain a repulsive force and energy of 2.3 pN (a carbon–carbon bond breaks at 3.7 nN) and 150 meV (3.6 eV is required to break a C–C bond), respectively. While the result shows that the force and energy is insufficient to break bonds, it is getting close to the energy level that is required to orient dipoles. PMMA electrets have three distinct polarization mechanisms with activation energies of 0.8, 2.1, and 2.4 eV.<sup>34</sup> The first two relate to the orientation of dipoles, while the last one relates to the required energy to relax trapped real charges. The lowest relaxation occurs at 0.8 eV and is associated to the reorientation of polar ester side groups by local motion around the C–C bond.<sup>35</sup> Our estimated energy level (150 meV) is below the threshold (0.8 eV) to cause mechanical reorientation of polar side groups or the diffusion (2.4 eV) of real charge. Some level of relaxation and charge diffusion inside the PMMA cannot be completely excluded at this point. However, dipole relaxation and charge diffusion inside the PMMA are unlikely to be the main mechanisms that can explain the large lateral broadening of the recorded surface potential distribution.

Third, the broadening could be induced by interference with the KFM tip during the measurement. In KFM it is required to apply an ac voltage between the scanning probe and the silicon substrate. Considering a 50 nm thick layer of PMMA and a typical 5 V potential modulation, we obtain a local electric field that is at least 1 V/10 nm and a force of 16 pN that acts on a single elementary charge within the PMMA layer which is four times larger than the repulsive force between two single elementary charges that are separated by 10 nm that was discussed in the previous paragraph. It is difficult to state if this additional factor is sufficient to cause diffusion. In practical experiments we observed a slight decay in the recorded charge level after prolonged scanning.

The discussion of the three mechanisms that could cause the broadening of the recorded surface potential illustrates that it is difficult to use KFM to determine the actual physical dimensions of the charge pattern or whether a lateral diffusion takes place at length scales below 100 nm. For similar charge patterns we have observed feature sizes in the potential distribution that range from 150 to 300 nm with different KFM probes. Such variations are only observed for electrode structures below 200 nm. Larger structures show a one to one comparison between contact area and the width of the KFM surface potential image. On the basis of our calculations and experimental observation, we conclude that the main limiting factor is the tip geometry and condition; however, lateral diffusion or relaxation of dipoles due to the strong electrostatic fields or screening by ions due to adsorbed surface water cannot be completely ruled out at this time.

Trapped surface charge finds a primary application in nanoxerographic printing. Figure 3 shows representative images of nanoxerographic printing of nanoparticles from the gas phase. The images show parallel lines and square shapes of 20–60 nm sized silver and germanium nanoparticles that are trapped at charged areas that have been deposited onto the substrate from the gas phase. The charge patterns were generated using the thin silicon electrodes shown in Figure 2. The width of the assembled lines of nanoparticles was 60 nm, which is in good agreement with the 50 nm wide lines on the thin silicon electrodes. This is the first result of this kind. The results suggest that nanoparticles may be used as a visual tool to resolve the lateral distribution of charge patterns at length scales below 100 nm.

We currently do not know what the ultimate resolution limit is. It may be limited only by the size of the particles as long as the electrostatic interaction is stronger than the Brownian motion. The kinetic energy due to the Brownian motion is 25 meV at room temperature. The ordering energy due to the trapped charge can be estimated by the recorded changes in the surface potential distribution ( $\Delta V = 1$  V). The energy gain between a charged and uncharged region, considering that the particles contain at least a single elementary charge, is at least 1 eV and more than 2 orders of magnitude bigger than the disordering energy due to Brownian motion.

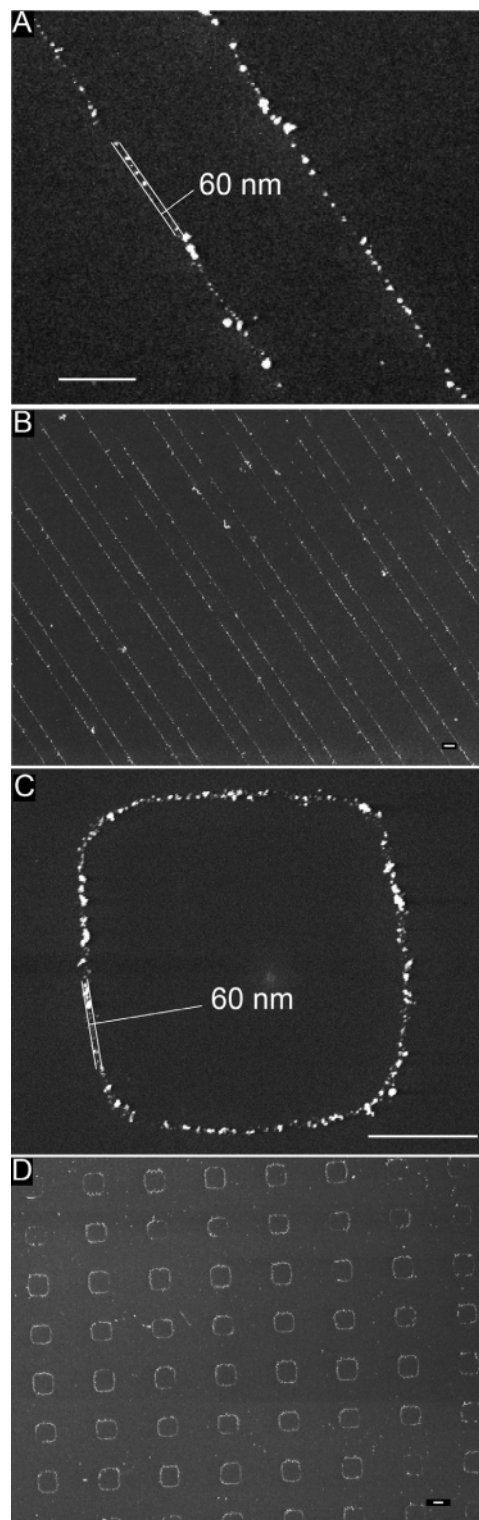


**Figure 3.** SEM images of 60 nm wide lines and squares consisting of (A, B) unoxidized silver nanoparticles and (C, D) oxidized germanium nanoparticles assembled using an evaporation system. The underlying charge was patterned with thin silicon electrodes containing 50 nm wide features extending from the surface. Scale bars are 1  $\mu$ m in length.

We also investigated the evolution of the assembly process as a function of deposition time. Using silver nanoparticles generated in the tube furnace at 1060 °C, we observed the formation of dendrites with increased assembly times. We

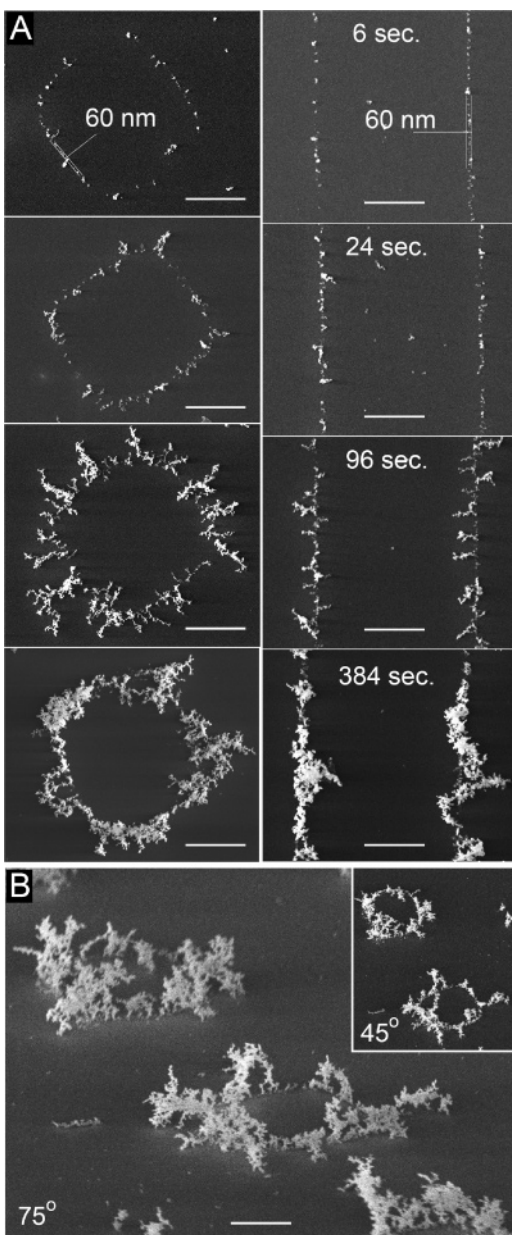


**Figure 4.** (A) SEM images of the progression of assembled silver nanoparticles on charge patterned squares and lines. The assembly time ranged from 6 to 384 s. For the 6-s assembly, 60 nm resolution was achieved. As assembly time increased, the particles grew along the field lines into fractal structures. (B) SEM image taken at a 75° angle of the fractal silver nanoparticle structures formed on the square charge patterned areas. The inset shows the same area at an angle of 45°. All scale bars are 1 μm in length.

have observed the dendritic growth patterns with similar metals such as indium, gallium, and gold although the growth times differ between metals and evaporation temperatures. Other materials such as iron oxide, graphitized carbon, iron beads, and silicon did not show this behavior. With the subclass of materials that form dendrites we observe an initial assembly that matches our charge patterned area. As we increase the assembly time, particles begin to attach to those assembled on the charge patterned substrate forming fractal type structures. Figure 4A shows how these patterns evolved over time in the case of silver nanoparticles. A high-

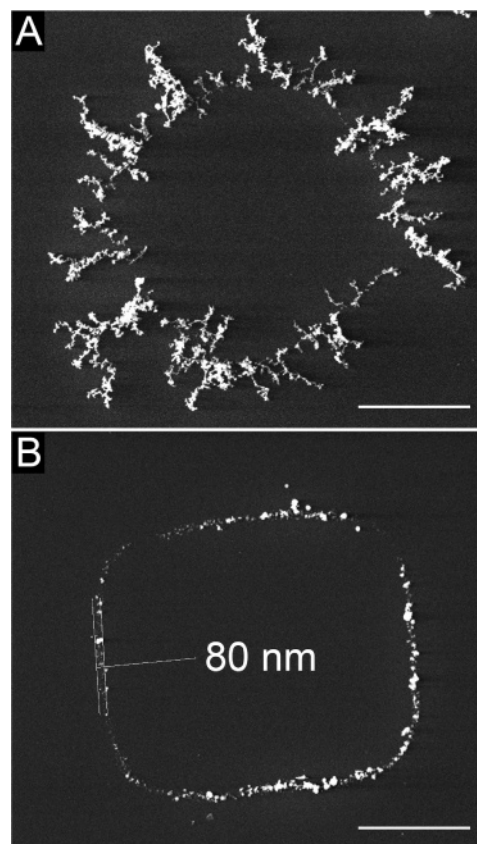


**Figure 5.** (A) SEM image of unoxidized silver nanoparticles assembled on a square charge pattern for 96 s. (B) SEM image of oxidized silver nanoparticles assembled on a square charge pattern for 96 s. Note the reduction and almost elimination of the fractal growth structures. Scale bars are 1 μm in length.

resolution line of assembled particles forms after 6–10 s. These particles act as attachment sites for new particles that are deposited from the gas phase. The fractal type patterns have a preferential orientation that is perpendicular to that of the charged lines, i.e., along the direction of the fringing field. Incoming particles follow the direction of the fringing field and attach preferentially at the end of an evolving “wire”. Figure 4B shows an angled view of the square shape patterns which illustrates that most of the “wires” extend into the half space. We currently do not understand the growth mechanism in detail but believe that the establishment of a conduction path would be required to transport the charge of incoming nanoparticles to the substrate surface. A conducting wire could amplify the underlying fringing field. The formation of these patterns is not likely if the assembled particles retain their charge and repel each other during the experiment.

To validate our conduction path hypothesis we oxidized the particles before assembly. A quenching flow of compressed air was attached to the exit of the furnace, allowing oxygen to mix with the flow of nanoparticles before they cooled and entered the assembly module. Figure 5 provides an example of the effects of the oxygen treatment on the assembly. The untreated silver nanoparticles evolved into large dendrite structures after 96 s (Figure 5A), while the oxygen-treated silver nanoparticles (Figure 5B) remained

dendrite free with the same assembly time. We have observed the reduction and often the elimination of the fractal growth by this method for several different materials. Figure 3C, for example, shows oxidized germanium nanoparticles assembled for 192 s onto square charge patterns with  $\sim 60$  nm resolution.

In conclusion, thin silicon provides a suitable, semiflexible material that can be used in electric nanocontact printing. Electrical nanocontacts can be formed that are as small as 50 nm by placing the nanostructured electrodes onto an electret surface. The nanocontacts can be used to inject charge into 50 nm sized areas. We observed an interesting mismatch between the lateral resolution of the recorded surface potential distribution (300 nm wide lines and rings), nanoparticle patterns (60 nm wide lines and rings), and electrode structures (50 nm wide lines and rings). Our hypothesis is that our Kelvin probe force microscope that is operated under ambient conditions is not capable of resolving the embedded charge patterns with sub-100-nm resolution. The highest resolution we have obtained so far is 60 nm; however, there appears to be no physical limitation to suggest that Coulomb force directed assembly cannot be used at the sub-10-nm length scale. While structures as small as 10 nm have been generated in bulk silicon,<sup>36</sup> they are not widely available. The current bottleneck preventing us from fabricating nanomaterial-based devices at desired locations is related to the level of control. For example to integrate novel devices such as nanoparticle transistors<sup>37</sup> and LEDs on a surface, we need to be able to adjust the number of particles that are being deposited as well as the interparticle spacing. We believe that it will be necessary to adjust the charge on the particle and substrate to gain control over the packing density and interparticle spacing.

**Acknowledgment.** The authors are pleased to acknowledge the financial support for the research by the National Science Foundation through the Integrative Graduate Education and Research Traineeship program (IGERT DGE-0114372), the Nanotechnology and Interdisciplinary Research Initiative (NIRT DMI-0304211), and Grant DMI-0217538.

## References

- Piner, R. D.; Zhu, J.; Xu, F.; Hong, S.; Mirkin, C. A. "Dip-pen" nanolithography. *Science (Washington, DC)* **1999**, *283* (5402), 661–663.
- Bullen, D.; Chung, S.-W.; Wang, X.; Zou, J.; Mirkin, C. A.; Liu, C. Parallel dip-pen nanolithography with arrays of individually addressable cantilevers. *Appl. Phys. Lett.* **2004**, *84* (5), 789–791.
- Baur, C.; Bugacov, A.; Koel, B. E.; Madhukar, A.; Montoya, N.; Ramachandran, T. R.; Requicha, A. A. G.; Resch, R.; Will, P. Nanoparticle manipulation by mechanical pushing: underlying phenomena and real-time monitoring. *Nanotechnology* **1998**, *9* (4), 360–364.
- de Gans, B.-J.; Duineveld, P. C.; Schubert, U. S. Inkjet printing of polymers: State of the art and future developments. *Adv. Mater. (Weinheim, Germany)* **2004**, *16* (3), 203–213.
- Magdassi, S.; Ben Moshe, M. Patterning of Organic Nanoparticles by Ink-jet Printing of Microemulsions. *Langmuir* **2003**, *19* (3), 939–942.
- Loo, Y.-L.; Willett, R. L.; Baldwin, K. W.; Rogers, J. A. Additive, nanoscale patterning of metal films with a stamp and a surface chemistry mediated transfer process: Applications in plastic electronics. *Appl. Phys. Lett.* **2002**, *81* (3), 562–564.
- Jeon, S.; Menard, E.; Park, J.-U.; Maria, J.; Meitl, M.; Zaumseil, J.; Rogers, J. A. Three-dimensional nanofabrication with rubber stamps and conformable photomasks. *Adv. Mater. (Weinheim, Germany)* **2004**, *16* (15), 1369–1373.
- Wright, W. M. D.; Chetwynd, D. G. Can charge writing aid nanotechnological manipulation. *Nanotechnology* **1998**, *9* (2), 133–142.
- Niemeyer, C. M.; Ceyhan, B.; Gao, S.; Chi, L.; Peschel, S.; Simon, U. Site-selective immobilization of gold nanoparticles functionalized with DNA oligomers. *Colloid Polym. Sci.* **2001**, *279* (1), 68–72.
- Rao, S. G.; Huang, L.; Setyawan, W.; Hong, S. Nanotube electronics: large-scale assembly of carbon nanotubes. *Nature (London)* **2003**, *425* (6953), 36–37.
- Yellen, B. B.; Friedman, G. Programmable assembly of heterogeneous colloidal particle arrays. *Adv. Mater.* **2004**, *16* (2), 111–115.
- Jacobs, H. O.; Whitesides, G. M. Submicrometer patterning of charge in thin-film electrets. *Science* **2001**, *291* (5509), 1763–1766.
- Jacobs, H. O.; Campbell, S. A.; Steward, M. G. Approaching NanoXerography: The use of Electrostatic Forces to Position Nanoparticles with 100 Nanometer Scale Resolution. *Adv. Mater.* **2002**, *14* (21), 1553–1557.
- Barry, C. R.; Steward, M. G.; Lwin, N. Z.; Jacobs, H. O. Printing nanoparticles from the liquid and gas phases using nanoxerography. *Nanotechnology* **2003**, *14* (10), 1057–1063.
- Barry, C. R.; Lwin, N. Z.; Zheng, W.; Jacobs, H. O. Printing nanoparticle building blocks from the gas-phase using nanoxerography. *Appl. Phys. Lett.* **2003**, *83*, 5527.
- Mesquida, P.; Stemmer, A. Attaching silica nanoparticles from suspension onto surface charge patterns generated by a conductive atomic force microscope tip. *Adv. Mater.* **2001**, *13* (18), 1395–1398.
- Naujoks, N.; Stemmer, A. Micro- and nanoxerography in liquids – controlling pattern definition. *Microelectron. Eng.* **2005**, *78*–79, 331–337.
- Krinke, T. J.; Fissan, H.; Deppert, K.; Magnusson, M. H.; Samuelson, L. Positioning of nanometer-sized particles on flat surfaces by direct deposition from the gas phase. *Appl. Phys. Lett.* **2001**, *78* (23), 3708–3710.
- Chothia, C.; Janin, J. Principles of protein–protein recognition. *Nature* **1975**, *256* (5520), 705–8.
- Dabrowski, M. J.; Chen, J. P.; Shi, H. Q.; Chin, W. C.; Atkins, W. M. Strategies for protein-based nanofabrication: Ni<sup>2+</sup>-NTA as a chemical mask to control biologically imposed symmetry. *Chem. Biol.* **1998**, *5* (12), 689–697.
- Braun, E.; Eichen, Y.; Sivan, U.; Benyoseph, G. Dna-templated assembly and electrode attachment of a conducting silver wire. *Nature* **1998**, *391* (6669), 775–778.
- Huang, Y.; Joo, S.; Duhon, M.; Heller, M.; Wallace, B.; Xu, X. Dielectrophoretic cell separation and gene expression profiling on microelectronic chip arrays. *Anal. Chem.* **2002**, *74* (14), 3362–3371.
- Winningham, T. A.; Gillis, H. P.; Chouto, D. A.; Martin, K. P.; Moore, J. T.; Douglas, K. Formation of ordered nanocluster arrays by self-assembly on nanopatterned Si(100) surfaces. *Surf. Sci.* **1998**, *406* (1–3), 221–228.
- Cui, Y.; Bjoerk, M. T.; Liddle, J. A.; Soennichsen, C.; Boussett, B.; Alivisatos, A. P. Integration of Colloidal Nanocrystals into Lithographically Patterned Devices. *Nano Lett.* **2004**, *4* (6), 1093–1098.
- Li, D.; Ouyang, G.; McCann, J. T.; Xia, Y. Collecting Electrospun Nanofibers with Patterned Electrodes. *Nano Lett.* **2005**, *5*, 913–916.
- Mueller, T.; Gerardino, A. M.; Schnelle, T.; Shirley, S. G.; Fuhr, G.; De Gasperis, G.; Leoni, R.; Bordoni, F. High-frequency electric-field trap for micron and submicron particles. *Nuovo Cimento della Societa Italiana di Fisica, D: Condensed Matter, Atomic, Molecular and Chemical Physics, Fluids, Plasmas, Biophysics* **1995**, *17D* (4), 425–432.
- Fudouzi, H.; Kobayashi, M.; Shinya, N. Assembling 100 nm scale particles by an electrostatic potential field. *J. Nanopart. Res.* **2001**, *3* (2–3), 193–200.
- Velev, O. D.; Prevo, B. G.; Bhatt, K. H. On-chip manipulation of free droplets. *Nature (London)* **2003**, *426* (6966), 515–516.
- Odom, T. W.; Love, J. C.; Wolfe, D. B.; Paul, K. E.; Whitesides, G. M. Improved pattern transfer in soft lithography using composite stamps. *Langmuir* **2002**, *18* (13), 5314–5320.
- Jacobs, H. O.; Knapp, H. F.; Muller, S.; Stemmer, A. Surface potential mapping – a qualitative material contrast in spm. *Ultramicroscopy* **1997**, *69* (1), 39–49.

- (31) Jacobs, H. O.; Leuchtman, P.; Homan, O. J.; Stemmer, A. Resolution and contrast in kelvin probe force microscopy. *J. Appl. Phys.* **1998**, *84* (3), 1168–1173.
- (32) Jacobs, H. O.; Stemmer, A. Measuring and modifying the electric surface potential distribution on a nanometre scale: A powerful tool in science and technology. *Surf. Interface Anal.* **1999**, *27* (5–6), 361–367.
- (33) Jackson, J. D. *Classical Electrodynamics*; Wiley: New York, 1975.
- (34) Perlman, M. M.; Editor, *Electrets: Charge Storage and Transport in Dielectrics*; Electrochemical Society: Princeton, NJ, 1973; 675 pp.
- (35) Mazur, K. More data about dielectric and electret properties of poly-(methyl methacrylate). *J. Phys. D: Appl. Phys.* **1997**, *30* (9), 1383–1398.
- (36) Xia, Y.; Rogers, J. A.; Paul, K. E.; Whitesides, G. M. Unconventional methods for fabricating and patterning nanostructures. *Chem. Rev.* **1999**, *99* (7), 1823–1848.
- (37) Ding, Y.; Dong, Y.; Campbell, S. A.; Jacobs, H. O.; Bapat, A.; Kortshagen, U.; Perrey, C.; Carter, C. B. Field-Effect Transistor Built with a Single-Crystal Si Nanoparticle. Proceedings of 2005 NSF DMII Grantees Conference, Scottsdale, Arizona, January 3–6, 2005. NL0511972